Numerical modelling of the evaporation of a sessile drop consisting in an aqueous solution of salt and a soluble protein

Javier Martínez Puig and Javier Rodríguez Rodríguez

Carlos III University of Madrid, SPAIN

September 6, 2024

1 Introduction

In this short document we describe the theoretical and numerical modeling of the evaporation and solute transport inside a sessile drop with a composition similar to that of saliva. The model is based on our own experimental observations, carried out both at UC3M and at UTwente (with Prof. A. Marín), and has the objective of helping us to explain the morphology of the solid residue observed after the drop water content has fully evaporated.

From Vejerano and Marr [1] we know that the main components of saliva are water, salt (NaCl) (9 mg/ml), the glycoprotein Mucin (3 mg/ml), and a pulmonary surfactant. To reproduce as faithfully as possible the respiratory-droplet while keeping the complexity within reasonable bounds, we model our drop as consisting of water, salt and glycoprotein. The surfactanct will be included by introducing a solutal Marangoni effect.

Moreover, although the liquid density is a function of the composition, we will treat the flow as incompressible. The only effect of the spatially- and time-varying density field will be through buoyancy forces. Treating the liquid as incompressible and only considering the effect of the density variations through buoyancy forces is denoted Boussinesq approximation (solutal, in our case).

Based on these observations, we introduce several hypothesis to make the problem tractable: axisymmetric flow, Stokes flow (i.e. we neglect fluid inertia), and contact line pinning.

2 Definition of the geometry

Inspired by our experimental observations, as well as those of others, we model the flow as axisymmetric. For this reason, the numerical domain on which we will solve

the equations, Ω, is two dimensional. The domain has two phases, the liquid phase Ω_D and the gas phase Ω_G, so $\Omega = \Omega_D \cup \Omega_G$. The boundaries of our domain are the gas far field Γ_F, the substrate Γ_{Sub}, the symmetry axis Γ_{Sym} and the interphase between the gas phase and the liquid phase Γ_I. We denote the contact angle of the droplet with the substrate as θ and the contact radius R_c. Consistently with out experiments, we assume that R_c is constant during the evaporation process, so θ evolves in time. The full geometry can be seen in figure 1.

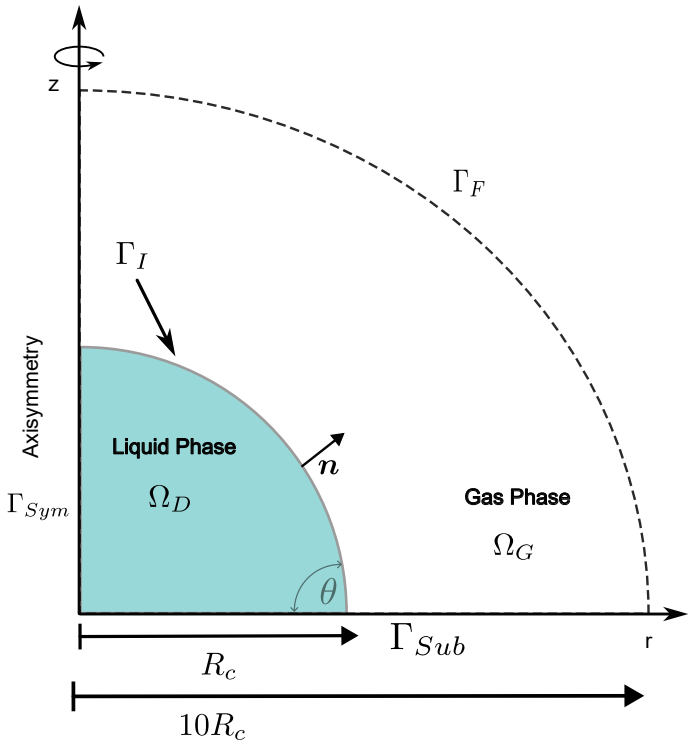

Fig. 1. Sketch of the mathematical domain Ω.

3 Transport model in the gas phase

In the gas phase we consider the diffusion-driven transport of vapor from the droplet into the air. When the droplet evaporates at a temperature far below the boiling point, and in the absence of forced or strong natural convection, the transport in the gas phase can be considered purely diffusive. Also, the evolution of the vapor concentration field can be treated as quasi-stationary since the diffusive time scale $D_{vap}/R_c^2 \sim 10^{-1}$ s is several orders of magnitude smaller than the droplet drying time $\rho_0 V_0/(4R_c D_{vap} C_s(1-H_r)) \sim 10^2$ s. Here, V_0 is the initial drop volume, ρ_0 the (constant) liquid density, D_{vap} the diffusivity of water vapor in air, C_s the saturation concentration, and H_r the relative humidity.

The saturation concentration of vapor in air is given by $C_s = p_v(T)/R^0 T$, where R^0 is the ideal gas constant and $p_v(T)$ the vapor pressure at a given temperature, which we compute using Antoine's law [2]:

$$p_v(T) = 10^5 \exp\left(11.68 - \frac{3816.44}{226.87 + T - 273.15}\right). \tag{1}$$

In this equation, the temperature is in Kelvin and the pressure value will be given in Pascals.

Under the above assumptions, the equation for the transport of vapor in the air reduces to the Laplacian

$$\nabla^{2^*} C^*_{vap} = 0 \text{ at } \Omega_G. \tag{2}$$

We use $*$ to denote the dimensional water vapor concentration and Nabla operator. We describe now the boundary conditions to integrate this equation. At the substrate and the symmetry axis we impose no flux of vapor:

$$\boldsymbol{\nabla}^* C^*_{vap} \cdot \boldsymbol{n} = 0 \text{ at } \Gamma_{Sub} \cup \Gamma_{Sym} \tag{3}$$

At the interphase between the liquid and the gas, thermodynamic equilibrium imposes

$$C^*_{vap} = C_s \, \chi(w_s) \text{ at } \Gamma_I. \tag{4}$$

Here, χ is the water activity. According to our experiments [3], for drops with salt and protein concentrations around their physiological values, the water activity depends only on the salt mass fraction w_s. To model the function $\chi(w_s)$ we use the polynomial interpolation of experimental data proposed by Mikhailov and coworkers [4].

Far away from the droplet we have

$$C^*_{vap} = C_s \, H_r \text{ at } \Gamma_F \tag{5}$$

Since we model the drop evaporation process as isothermal, it makes sense to use the vapor saturation concentration C_s to nondimensionalize the vapor concentration C^*_{vap}. Doing so, the dimensionless equations for the transport of vapor in air result:

$$\begin{aligned}
\nabla^2 C_{vap} &= 0 \text{ at } \Omega_G && (6)\\
\boldsymbol{\nabla} C_{vap} \cdot \boldsymbol{n} &= 0 \text{ at } \Gamma_{Sub} \cup \Gamma_{Sym} && (7)\\
C_{vap} &= \chi(w_s) \text{ at } \Gamma_I && (8)\\
C_{vap} &= H_r \text{ at } \Gamma_F. && (9)
\end{aligned}$$

Notice that we omit the $*$ in the dimensionless versions of ∇^* and C^*_{vap}.

4 Evaporation Rate

We solve the vapor concentration in the gas phase in order to compute the evaporation rate $\boldsymbol{J}^*$. There are analytical solutions for the evaporation rate in the case of a pure water droplet, but in our case the coupling of the evaporation rate with the salt mass fraction through the water activity at the surface makes necessary the numerical computation of $\boldsymbol{J}^*$. The evaporation rate is defined as

$$\boldsymbol{J}^* = -D_{vap} \boldsymbol{\nabla}^* C^*_{vap}, \tag{10}$$

in dimensionless form this is

$$\boldsymbol{J} = -\frac{D_{vap} C_s}{R_c J_c} \boldsymbol{\nabla} C_{vap} \tag{11}$$

where J_c is a characteristic scale for the evaporation rate. As we will see, a convenient choice is $J_c = \rho_0 D_s / R_c$. In dimensionless form we have

$$\boldsymbol{J} = -D\lambda \boldsymbol{\nabla} C_{vap} \tag{12}$$

where $\lambda = C_s/\rho_0$ and $D = D_{vap}/D_s$. Here D_s is the diffusivity of salt in water.

5 Transport of salt and protein inside the liquid phase

5.1 Transport equations

We will characterize the composition field using the mass fractions, w_w, w_s, and w_p, where the subindexes stand respectively for water, salt and protein. Since these three mass fractions must obey $w_w + w_s + w_p = 1$, we need to write advection-diffusion transport equations for only two of them, namely salt and protein.

The reason to choose these two components and not water is that, in the dilute concentration regime, the diffusive mass flux of protein and salt can be assumed to follow Fick's law. This is not so evident when we speak of water. In fact, applying mass conservation to a fluid particle, we find that there can be no net diffusive flux of mass. This implies that the three diffusive masses must add up to zero, in other words, that the diffusive mass flux of water should be

$$\boldsymbol{J}_w^* = -D_s \boldsymbol{\nabla}^* w_s - D_p \boldsymbol{\nabla}^* w_p. \tag{13}$$

If we assume that water diffusion is also Fickean, we could write

$$\boldsymbol{J}_w^* = -D_w \boldsymbol{\nabla}^* w_w. \tag{14}$$

Combining (13) and (14), and using $w_w = 1 - w_s - w_p$, we get

$$(D_s - D_w) \boldsymbol{\nabla}^* w_s + (D_p - D_w) \boldsymbol{\nabla}^* w_p = 0. \tag{15}$$

This equation implies that the iso-concentration curves of salt and protein must be parallel everywhere. This is clearly not what we observe in experiments. Furthermore, it is easy to conceive a carefully prepared initial concentration field where this condition is violated. For example, think of a water container with a vertical stratification of salt on which horizontal free surface we carefully deposit, at two nearby locations, two drops of water with different protein concentrations. This would create a horizontal gradient of protein concentration, whilst the salt concentration gradient should be nearly vertical, in clear violation of equation (15). Besides these arguments, it is also reasonable to assume that water diffusion is not Fickean as, if salt and protein are diluted, then water cannot be.

In summary, we have the two following advection-diffusion transport equations for salt and protein:

$$\partial_{t^*} w_p + \boldsymbol{v}^* \cdot \boldsymbol{\nabla}^* w_p = D_p \nabla^{2^*} w_p \tag{16}$$

$$\partial_{t^*} w_s + \boldsymbol{v}^* \cdot \boldsymbol{\nabla}^* w_s = D_s \nabla^{2^*} w_s. \tag{17}$$

5.2 Boundary conditions

We present now the boundary conditions for these two equations. At the substrate and at the symmetry axis we have a no-flux boundary condition

$$\boldsymbol{\nabla}^* w_p \cdot \boldsymbol{n} = 0 \text{ at } \Gamma_{Sym} \cup \Gamma_{Sub} \tag{18}$$

$$\boldsymbol{\nabla}^* w_s \cdot \boldsymbol{n} = 0 \text{ at } \Gamma_{Sym} \cup \Gamma_{Sub}. \tag{19}$$

At the drop-air interphase the water mass flux must balance the evaporation rate computed by solving the vapor transport at the air side, $J^* = \boldsymbol{J^*} \cdot \boldsymbol{n}$:

$$w_w(\boldsymbol{v}^* - \boldsymbol{v_I}^*) \cdot \boldsymbol{n} - \boldsymbol{J}_w^* \cdot \boldsymbol{n} = \frac{J^*}{\rho_0} \text{ at } \Gamma_I, \tag{20}$$

where $\boldsymbol{v_I}^*$ is the velocity of the drop free surface. Moreover, since the concentration of salt and protein in the gas phase is zero,

$$w_p(\boldsymbol{v}^* - \boldsymbol{v_I}^*) \cdot \boldsymbol{n} - D_p \boldsymbol{\nabla}^* w_p \cdot \boldsymbol{n} = 0 \text{ at } \Gamma_I \tag{21}$$

$$w_s(\boldsymbol{v}^* - \boldsymbol{v_I}^*) \cdot \boldsymbol{n} - D_s \boldsymbol{\nabla}^* w_s \cdot \boldsymbol{n} = 0 \text{ at } \Gamma_I. \tag{22}$$

We can sum the three boundary conditions and, using $w_w + w_s + w_p = 1$ once more and that the diffusive mass fluxes must sum zero, we arrive to the kinematic boundary condition

$$(\boldsymbol{v^*} - \boldsymbol{v_I^*}) \cdot \boldsymbol{n} = \frac{J^*}{\rho_0} \text{ at } \Gamma_I. \tag{23}$$

This equation will be used to solve for the evaporation-driven normal component of the interphase velocity, $\boldsymbol{v_I}^*$. It also lets us rewrite the boundary conditions for salt and protein mass fractions at the interphase as

$$D_p \boldsymbol{\nabla}^* w_p \cdot \boldsymbol{n} = \frac{J^* w_p}{\rho_0} \text{ at } \Gamma_I \tag{24}$$

$$D_s \boldsymbol{\nabla}^* w_s \cdot \boldsymbol{n} = \frac{J^* w_s}{\rho_0} \text{ at } \Gamma_I. \tag{25}$$

5.3 Non-dimensionalization

To nondimensionalize our equations we choose

$$\boldsymbol{x} = \frac{\boldsymbol{x^*}}{R_c},\ \boldsymbol{v} = \boldsymbol{v}^* \frac{R_c}{D_s},\ t = t^* \frac{D_s}{R_c^2}. \tag{26}$$

Now we can justify the choice of $J_c = \rho D_s / R_c$ because it leads to a kinematic boundary condition free of parameters,

$$(\boldsymbol{v} - \boldsymbol{v_I}) \cdot \boldsymbol{n} = J. \tag{27}$$

Applying the proposed non-dimensionalization to the rest of equations and boundary conditions we have

$$\partial_t w_p + \boldsymbol{v} \cdot \boldsymbol{\nabla} w_p = \mathcal{D} \nabla^2 w_p \text{ at } \Omega_D \tag{28}$$

$$\partial_t w_s + \boldsymbol{v} \cdot \boldsymbol{\nabla} w_s = \nabla^2 w_s \text{ at } \Omega_D \tag{29}$$

$$\boldsymbol{\nabla} w_p \cdot \boldsymbol{n} = 0 \text{ at } \Gamma_{Sym} \cup \Gamma_{Sub} \tag{30}$$

$$\boldsymbol{\nabla} w_s \cdot \boldsymbol{n} = 0 \text{ at } \Gamma_{Sym} \cup \Gamma_{Sub} \tag{31}$$

$$\boldsymbol{\nabla} w_p \cdot \boldsymbol{n} = \frac{J\, w_p}{\mathcal{D}} \text{ at } \Gamma_I \tag{32}$$

$$\boldsymbol{\nabla} w_s \cdot \boldsymbol{n} = J w_s \text{ at } \Gamma_I. \tag{33}$$

We have introduced the diffusivity ratio $\mathcal{D} = D_p/D_s$. To compute the mass fraction of water, whenever needed, we can use $w_w = 1 - w_p - w_s$.

6 Hydrodynamic equations

6.1 Continuity Equation

In what follows, we will denote the composition-dependent liquid density by ρ^*. The evolution of the density is given by the continuity equation

$$\partial_{t^*} \rho^* + \boldsymbol{\nabla^*} \cdot (\rho^* \boldsymbol{v^*}) = 0 \tag{34}$$

Until this moment we have considered the density as a constant, ρ_0 but, in fact, the density depends on the composition. That is, on the mass fractions w_s and w_p. For dilute solutions, the density can be modeled as a linear function of both mass fractions [5], [6]:

$$\rho^* = \rho_0 + \Delta\rho^* = \rho_0 + \rho_s w_s + \rho_p w_p. \tag{35}$$

However, since $\Delta\rho^*/\rho_0 \ll 1$ we just retain the term ρ_0 in all the previous equations. An exception to this is the gravity term.

Taking the density as constant everywhere except in the gravity term is called the Boussinesq approximation, solutal Boussinesq approximation in our case. This approximation has been customarily used in droplet modelization [7], [8]. As an example of why we have been able to neglect density variations in the previous equations, let us explain the non-dimensionalization of the continuity equation. Using the same non-dimensionalization for the time, length (and thus velocity) used before, continuity reads

$$\partial_t(\rho_0 + \rho_s w_s + \rho_p w_p) + \boldsymbol{\nabla} \cdot ((\rho_0 + \rho_s w_s + \rho_p w_p)\boldsymbol{v}) = 0 \tag{36}$$

Dividing by ρ_0 we have that

$$\partial_t \left(1 + \frac{\rho_s w_s + \rho_p w_p}{\rho_0}\right) + \boldsymbol{\nabla} \cdot \left(\left(1 + \frac{\rho_s w_s + \rho_p w_p}{\rho_0}\right)\boldsymbol{v}\right) = 0 \tag{37}$$

Then as $(\rho_s w_s + \rho_p w_p)/\rho_0 \ll 1$ during the whole evaporation,

$$\boldsymbol{\nabla} \cdot \boldsymbol{v} = 0. \tag{38}$$

We have arrived at the continuity equation of an incompressible flow which is typical of the Boussinesq approximation.

6.2 Momentum Equation

The momentum equation for an incompressible fluid reads

$$\rho^*(\partial_t \boldsymbol{v^*} + \boldsymbol{v^*} \cdot \boldsymbol{\nabla^*} \boldsymbol{v^*}) = -\boldsymbol{\nabla^*} p^* + \boldsymbol{\nabla^*} \cdot (\mu^*(\boldsymbol{\nabla v^*} + \boldsymbol{\nabla} \boldsymbol{v^{*T}})) - \rho^* g \boldsymbol{e_z}. \tag{39}$$

Our non-dimensionalization, consistent with the one already used in the previous sections, will be

$$t = \frac{D_s}{R_c^2} t^*,\ \boldsymbol{x} = \frac{\boldsymbol{x^*}}{R_c},\ \boldsymbol{v} = \boldsymbol{v}^* \frac{R_c}{D_s},\ \mu = \frac{\mu^*}{\mu_w},\ P = \frac{R_c^2}{\mu_w D_s}(p^* + \rho_0 g z^*) \tag{40}$$

where μ_w is the viscosity of pure water and P is the dimensionless reduced pressure. The characteristic pressure $\Delta p_c = \mu_w D_s / R_c^2$ has been chosen because the pressure gradient should be of the same order than the viscous stresses. Applying the non-dimensionalitation we have

$$\begin{aligned} \frac{(\rho_0 + \rho_s w_s + \rho_p w_p) D_s}{\mu_w}(\partial_t \boldsymbol{v} \ &+ \ \boldsymbol{v} \cdot \boldsymbol{\nabla v}) = \\ &= \ -\boldsymbol{\nabla} P + \nabla \cdot (\mu(\boldsymbol{\nabla v} + \boldsymbol{\nabla} \boldsymbol{v}^T)) - \frac{R_c^3 g}{\mu_w D_s}(\rho_s w_s + \rho_p w_p) g \boldsymbol{e_z}. \end{aligned} \tag{41}$$

Applying again $\Delta\rho^*/\rho_0 \ll 1$ we have

$$Sc^{-1}(\partial_t \boldsymbol{v} + \boldsymbol{v} \cdot \boldsymbol{\nabla v}) = -\boldsymbol{\nabla} P + \boldsymbol{\nabla} \cdot (\mu(\boldsymbol{\nabla v} + \boldsymbol{\nabla} \boldsymbol{v}^T)) - Ra\, \rho\, \boldsymbol{e_z}, \tag{42}$$

where $Sc = \mu_w / D_s \rho_0$ is the Schmidt number, $Ra = R_c^3 g \rho_s / \mu_w D_s$ the Rayleigh number, and $\rho = (w_s + \rho_p / \rho_s\, w_p)$ a dimensionless density variation.

For our problem, $Sc > 10^3$, but we can only neglect inertia if the Reynolds number $Re = \rho_0 v_c R_c / \mu_w$ is also small [7]. We have used D_s/R_c for the non-dimensionalization of the velocity to leave the advection-diffusion equations free of parameters, but that does not mean that we expect velocities to be of this order. To confirm that we can neglect the inertial terms when compared to the viscous ones we need to estimate the characteristic velocity of our problem to build a Reynolds number. The dominant flow can be capillary or Marangoni-driven. In the case of capillary flow, the characteristic velocity (avoiding the singularity at the end of the evaporation) is $v_{Ca} \sim D_{vap} C_s (1 - H_r)/R_c \rho_0 \sim 1$ µm/s. In the case of Marangoni flow the characteristic velocity is given by $v_{Ma} \sim \Delta\gamma/\mu \sim (\mathrm{d}\gamma/\mathrm{d}w_s)\Delta w_s/\mu$. The value $\mathrm{d}\gamma/\mathrm{d}w_s$ is not easy to measure experimentally because of the contamination of the interface (and in our case because of the presence of protein). This is indeed a point of active discussions. The discrepancy between the magnitude measured in static conditions and that inferred from Marangoni flow measurements differ in three orders of magnitude! [9]. Indeed this is why, to compared with experiments, we plan to fit the value of $\mathrm{d}\gamma/\mathrm{d}w_s$ with our own experiments. Nevertheless we know from experiments

that $v_{Ma} \sim 100$ µm/s at most. We can then neglect inertia because in the worst case $Re \sim 10^{-2}$. In contrast with this $Ra \sim 10^6$ so we should keep buoyancy forces in the equations. This is the reason why we have applied the solutal Boussinesq approximation: changes in density are only relevant in the buoyancy forces, which only appear in the momentum equation. It is noteworthy to mention that the dimensionless density ρ is much smaller than unity, so having $Ra \sim 10^6$ does not mean that buoyancy forces are going to be dominant when we compare them with Marangoni forces.

Finally, the dimensionless momentum equation reads

$$\boldsymbol{\nabla} \cdot \overline{\overline{\tau}} - Ra\, \rho\, \boldsymbol{e_z} = 0, \tag{43}$$

where $\overline{\overline{\tau}} = -P\mathcal{I} + \mu(\boldsymbol{\nabla v} + \boldsymbol{\nabla v}^T)$ is the dimensionless stress tensor defined using the reduced pressure P.

6.3 Boundary conditions

At the symmetry axis we impose symmetry conditions

$$v_r = 0, \ \frac{\partial v_z}{\partial r} = 0 \text{ at } \Gamma_{Sym}. \tag{44}$$

At the substrate we have no slip boundary condition

$$\boldsymbol{v} = 0 \text{ at } \Gamma_{Sub}. \tag{45}$$

At the interphase we have the kinematic boundary condition already derived in the previous section which in dimensionless form results

$$(\boldsymbol{v} - \boldsymbol{v_I}) \cdot \boldsymbol{n} = J, \text{ at } \Gamma_I. \tag{46}$$

This equation is needed to compute the interphase as part of our solution. However, this condition only gives the normal component of the interphase velocity, so another equation is needed that includes the tangential velocity component. This is going to be the stress condition [7].

To perform a stress balance at the drop interphase we need to introduce surface tension γ^*, which is a measure of the free energy per unit area. Thus, an increase in the area of the interphase requires an increase in the free energy of the system. In a macroscopic mechanical theory, the only way to include the rate of work required to change the interphase area is to assume the existence of a force per unit length that acts at the edges of an interfacial element [10]. So the force equilibrium condition on an arbitrary surface element $A \in \Gamma_I$ with $C = \partial A$ is

$$\int_A (\tau_g^* - \tau_l^*) \cdot \boldsymbol{n}\, \mathrm{d}A + \int_C \gamma^*\, \boldsymbol{t}\, \mathrm{d}C = 0, \tag{47}$$

where τ_α is the stress tensor of phase α and $\boldsymbol{t}$ is a orthogonal vector to $\boldsymbol{n}$. This tensor has to account for both the dynamic and hydrostatic pressure, so we use p instead of P. We assume zero velocity and uniform pressure in the gas phase, which simplifies the above equation

$$-\int_A \tau^* \cdot \boldsymbol{n}\,\mathrm{d}A + \int_C \gamma^*\,\boldsymbol{t}\,\mathrm{d}C = 0. \tag{48}$$

Here we have dropped the subindex in the stress tensor, as it is only non-zero in the liquid phase. We can rewrite the curvilinear integral equation using the generalized Stokes theorem,

$$\int_C \gamma^*\,\boldsymbol{t}\,\mathrm{d}C = \int_A \boldsymbol{\nabla_t}^*\gamma^*\,\mathrm{d}A - \int_A \gamma^*\,(\boldsymbol{\nabla}^* \cdot \boldsymbol{n})\boldsymbol{n}\,\mathrm{d}A, \tag{49}$$

where $\boldsymbol{\nabla}^* \cdot \boldsymbol{n}$ is the curvature of the surface and $\boldsymbol{\nabla_t}^* = \boldsymbol{\nabla}^* - (\boldsymbol{n} \cdot \boldsymbol{\nabla}^*)\boldsymbol{n}$ is the component of the gradient operator in the local plane of the interphase, also called surface gradient operator. Using the localization theorem our stress condition at the interphase results

$$-\overline{\overline{\tau}}^* \cdot \boldsymbol{n} = \gamma^*(\boldsymbol{\nabla}^* \cdot \boldsymbol{n})\boldsymbol{n} - \boldsymbol{\nabla_t}^*\gamma^* + \rho_0 g z^* \boldsymbol{n}. \tag{50}$$

Notice that the hydrostatic pressure appears on the right-hand side of the equation, as we adopt here the definition of the stress tensor the reduced pressure. Furthermore, we assume that surface tension depends linearly on the concentration of salt $\gamma^* = \gamma_0 + \gamma_s w_s$. Then in dimensionless form the stress condition is

$$-\overline{\overline{\tau}} \cdot \boldsymbol{n} = Ca^{-1}(\boldsymbol{\nabla} \cdot \boldsymbol{n} + Bo\, z)\boldsymbol{n} - Ma\boldsymbol{\nabla_t} w_s. \tag{51}$$

where $Ca = \mu_w D_s/\gamma_0 R_c$ is the capillary number, $Ma = \gamma_s R_c/\mu_w D_s$ the Marangoni number, and $Bo = \rho g R_c^2/\gamma_0$ the Bond number.

6.4 Summary of equations and boundary conditions

To summarize, the hydrodynamic equations in the droplet are

$$\boldsymbol{\nabla} \cdot \boldsymbol{v} = 0, \text{ at } \Omega_D. \tag{52}$$

$$\boldsymbol{\nabla} \cdot \overline{\overline{\tau}} - Ra\,\rho\,\boldsymbol{e_z} = 0, \text{ at } \Omega_D \tag{53}$$

$$v_r = 0, \ \frac{\partial v_z}{\partial r} = 0 \text{ at } \Gamma_{Sym} \tag{54}$$

$$\boldsymbol{v} = 0, \text{ at } \Gamma_{Sub} \tag{55}$$

$$(\boldsymbol{v} - \boldsymbol{v_I}) \cdot \boldsymbol{n} = J, \text{ at } \Gamma_I \tag{56}$$

$$-\overline{\overline{\tau}} \cdot \boldsymbol{n} = Ca^{-1}(\boldsymbol{\nabla} \cdot \boldsymbol{n} + Boz)\boldsymbol{n} - Ma\boldsymbol{\nabla_t} w_s \text{ at } \Gamma_I. \tag{57}$$

An scheme of the model can be seen in figure 2.
This model accounts for the complexity of a respiratory droplet but has been kept as general as possible. Indeed it can be useful to study other ternary mixture droplets, where the solutal Boussinesq approximation can be applied $\Delta\rho^*/\rho^* \ll 1$ and inertia can be neglected. This happens in a wide variety of applications [7]. The particularities of the system can be introduced via the dimensionless viscosity and density, and the dimensionless numbers.

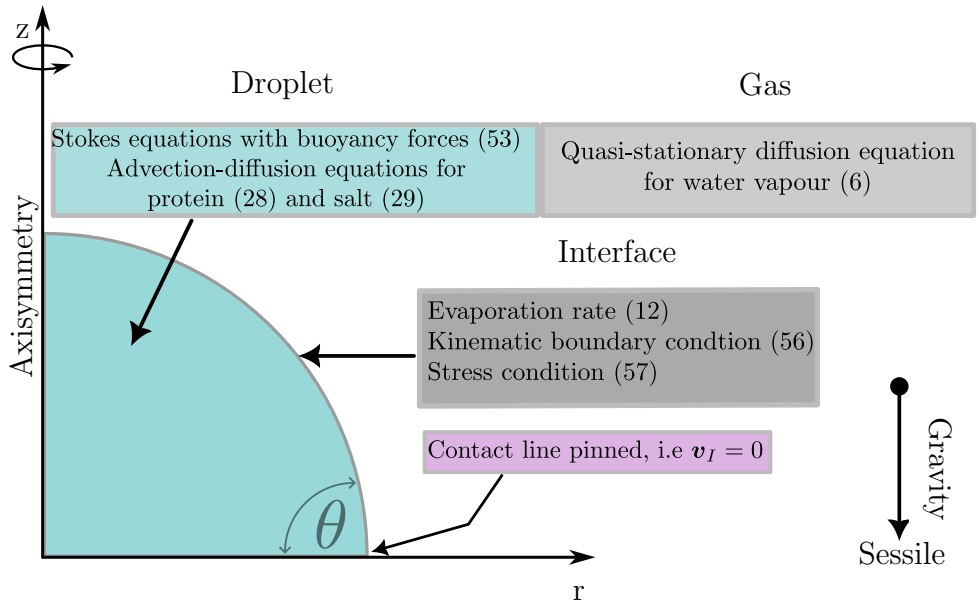

Fig. 2. Sketch of the model, detailing which equations are applied in the different domains and boundaries.

7 Numerical scheme

Since the very beginning of the study of sessile droplets evaporation [11] some analytical solutions have been derived to compute, not only the evaporation rate, but also the flow inside the drop. They are based on lubrication theory, which can be applied when we the geometry is slender, i.e., $h \ll R_c$. This approximation could be valid for $\theta \leq 30°$, but it does not give good results for higher contact angles, so we cannot use this approximation to solve our model. Indeed, in our experiments we need to use rather hydrophobic substrates which yield initial contact angles $\theta_0 \sim 90°$. Another, and perhaps more important, reason to not look for an analytical solution of our problem is the highly-coupled system we have, in which the mixture properties depend directly on protein and salt mass fraction.

Our approach to solve the system of equations is the numerical integration of the model's equations using a Finite Element Method (FEM), which is a methodology to spatially discretize partial differential equations and is amenable to be used in complex geometries. For doing this we are going to use the commercial solver Comsol [12]. As Comsol can be some sort of black box, the implementation of the equations will be done using the "Mathematics Module", which allows us to directly introduce our equations in weak form.

8 Weak formulation of the problem

We derive here the weak form of the incompressible Stokes equations with buoyancy forces (52), (53), and one of the advection-diffusion equations (e.g. for salt (29)) for sake of brevity. The weak formulation of the other advection-diffusion equation (28) and of the diffusive transport in the gas phase (6) are analogous to the the one derived here for the advection-diffusion equation of salt transport.

8.1 Advection-diffusion transport equation for a solute

We are set to obtain the weak form of the following problem

$$\partial_t w_s + \boldsymbol{v} \cdot \boldsymbol{\nabla} w_s = \nabla^2 w_s \text{ at } \Omega_D \tag{58}$$
$$\boldsymbol{\nabla} w_s \cdot \boldsymbol{n} = 0 \text{ at } \Gamma_{Sym} \cup \Gamma_{Sub} \tag{59}$$
$$\boldsymbol{\nabla} w_s \cdot \boldsymbol{n} = J w_s \text{ at } \Gamma_I \tag{60}$$

We start by multiplying equation (58) by an arbitrary test function $\hat{w}_s$ of some functional space, to be determined later, and integrating in the whole domain so we get

$$\int_{\Omega_D} \left[\partial_t w_s \hat{w}_s + \boldsymbol{v} \cdot \boldsymbol{\nabla} w_s \hat{w}_s - \nabla^2 w_s \hat{w}_s\right] \mathrm{d}\Omega_D = 0. \tag{61}$$

We can apply Green's theorem to the last integrand and obtain

$$\int_{\Omega_D} \left[\partial_t w_s \hat{w}_s + \boldsymbol{v} \cdot \boldsymbol{\nabla} w_s \hat{w}_s + \boldsymbol{\nabla} w_s \cdot \boldsymbol{\nabla} \hat{w}_s\right] \mathrm{d}\Omega_D - \int_{\Gamma_D} \boldsymbol{\nabla} w_s \cdot \boldsymbol{n}\, \hat{w}_s \mathrm{d}\Gamma_D = 0. \tag{62}$$

Applying the boundary conditions in the boundary integral we finally get

$$\int_{\Omega_D} \left[\partial_t w_s \hat{w}_s + \boldsymbol{v} \cdot \boldsymbol{\nabla} w_s \hat{w}_s + \boldsymbol{\nabla} w_s \cdot \boldsymbol{\nabla} \hat{w}_s\right] \mathrm{d}\Omega_D - \int_{\Gamma_D} J w_s \hat{w}_s \mathrm{d}\Gamma_I = 0. \tag{63}$$

For the integrals to be well posed we see that the test and solution functions must be at least $H^1(\Omega_D)$, this means w_s and $\hat{w}_s$ and their first spatial derivatives must be $L^2(\Omega_D)$, i.e square integrable. Also the temporal derivative of w_s must be $L^2([0, t_f])$ where t_f is the final time of the simulation.

8.2 Hydrodynamic equations

In this subsection we will derived the weak form of

$$\boldsymbol{\nabla} \cdot \boldsymbol{v} = 0, \text{ at } \Omega_D. \tag{64}$$
$$\boldsymbol{\nabla} \cdot \overline{\overline{\tau}} - Ra\, \rho\, \boldsymbol{e_z} = 0, \text{ at } \Omega_D \tag{65}$$
$$v_r = 0, \ \frac{\partial v_z}{\partial r} = 0 \text{ at } \Gamma_{Sym} \tag{66}$$
$$\boldsymbol{v} = 0, \text{ at } \Gamma_{Sub} \tag{67}$$
$$(\boldsymbol{v} - \boldsymbol{v_I}) \cdot \boldsymbol{n} = J, \text{ at } \Gamma_I \tag{68}$$
$$-\overline{\overline{\tau}} \cdot \boldsymbol{n} = Ca^{-1}(\boldsymbol{\nabla} \cdot \boldsymbol{n} + Boz)\boldsymbol{n} - Ma \boldsymbol{\nabla_t} w_s \text{ at } \Gamma_I. \tag{69}$$

The continuity equation is scalar and the momentum equation is a vector. We also have a vector unknown, the velocity, and a scalar unknown, the pressure. So the scalar test function $\hat{P}$ should be in the same function space as the pressure, and the vector test function $\hat{\boldsymbol{v}}$ in the same space as the velocity. Multiplying continuity equation by the scalar test function and integrating in the droplet domain we have

$$\int_{\Omega_D} (\boldsymbol{\nabla} \cdot \boldsymbol{v})\, \hat{P}\, \mathrm{d}\Omega_D = 0. \tag{70}$$

We can pass the derivative from the velocity to the scalar test function but, as in the momentum equation the pressure needs to be in the space $L^2(\Omega_D)$, is less requiring to keep the formulation like this. Also, applying Green's theorem to the integral will yield a boundary integral in which we should say something about the boundary conditions for the pressure. As this is not required for the model, which does not have boundary conditions on the pressure, the commonly adopted solution is to keep the formulation of the continuity equation with the derivative in the velocity.

For the Momentum equation we do the dot product of our equation with a vector test function $\hat{\boldsymbol{v}}$ and then integrate in the droplet domain to get

$$\int_{\Omega_D} \left[\boldsymbol{\nabla} \cdot \overline{\overline{\tau}} \cdot \hat{\boldsymbol{v}} - Ra\, \rho\, \boldsymbol{e_z} \cdot \hat{\boldsymbol{v}}\right] \mathrm{d}\Omega_D = 0 \tag{71}$$

We can rewrite the first integrand through the identity

$$\boldsymbol{\nabla} \cdot (\overline{\overline{\tau}} \cdot \hat{\boldsymbol{v}}) = (\boldsymbol{\nabla} \cdot \overline{\overline{\tau}}) \cdot \hat{\boldsymbol{v}} + \overline{\overline{\tau}}^T : \boldsymbol{\nabla}\hat{\boldsymbol{v}} = (\boldsymbol{\nabla} \cdot \overline{\overline{\tau}}) \cdot \hat{\boldsymbol{v}} + \overline{\overline{\tau}} : \boldsymbol{\nabla}\hat{\boldsymbol{v}}, \tag{72}$$

where we have used the symmetry of the stress tensor. We have then

$$\int_{\Omega_D} \left[\boldsymbol{\nabla} \cdot (\overline{\overline{\tau}} \cdot \hat{\boldsymbol{v}}) - \overline{\overline{\tau}} : \boldsymbol{\nabla}\hat{\boldsymbol{v}} - Ra\, \rho\, \boldsymbol{e_z} \cdot \hat{\boldsymbol{v}}\right] \mathrm{d}\Omega_D = 0. \tag{73}$$

Finally, applying Gauss divergence theorem we arrive at

$$\int_{\Omega_D} \left[-\overline{\overline{\tau}} : \boldsymbol{\nabla}\hat{\boldsymbol{v}} - Ra\, \rho\, \boldsymbol{e_z} \cdot \hat{\boldsymbol{v}}\right] \mathrm{d}\Omega_D + \int_{\Gamma_D} \boldsymbol{n} \cdot \overline{\overline{\tau}} \cdot \hat{\boldsymbol{v}}\, \mathrm{d}\Gamma_D = 0. \tag{74}$$

Applying then the stress boundary condition (57) and that the stresses normal to the boundary should be zero in the symmetry axis, we have that

$$\int_{\Omega_D} \left[\overline{\overline{\tau}} : \boldsymbol{\nabla}\hat{\boldsymbol{v}} + Ra\, \rho\, \boldsymbol{e_z} \cdot \hat{\boldsymbol{v}}\right] \mathrm{d}\Omega_D + \int_{\Gamma_I} \left[Ca^{-1}(\boldsymbol{\nabla} \cdot \boldsymbol{n} + Boz)\boldsymbol{n} - Ma\boldsymbol{\nabla_t} w_s\right] \cdot \hat{\boldsymbol{v}}\, \mathrm{d}\Gamma_I \tag{75}$$
$$- \int_{\Gamma_{Sub}} \boldsymbol{n} \cdot \overline{\overline{\tau}} \cdot \hat{\boldsymbol{v}}\, \mathrm{d}\Gamma_{Sub} = 0.$$

For the integrals to be well posed we need for the pressure to be just square integrable, and for the velocity that the first derivatives are also square integrable, this is P and $\hat{P}$ should be in $L^2(\Omega_D)$ and $\boldsymbol{v}$ and $\hat{\boldsymbol{v}}$ in $\boldsymbol{H}^1(\Omega_D)$. Theoretically we can choose the velocity test functions to be in the functional space $\boldsymbol{W} = \left\{\hat{\boldsymbol{v}} \in \boldsymbol{H}^1(\Omega_D) : \hat{\boldsymbol{v}} = 0 \text{ at } \Gamma_{Sub}\right\}$ so the last integral will vanish in equation (75). These is not possible when working in Comsol as we can specify the element and order we want to use to discretize our equations but we can not create a functional basis for our element such that some of the boundary conditions are fulfilled by this functional basis. So the boundary conditions that does not appear in the integral contribution from the boundary need to be imposed via Lagrange multipliers.

9 Practical implementation in Comsol

9.1 Geometry, Mesh and Discretization

One of the properties of the problem we are modelling is the axisymmetry. These allow us, using cylindrical coordinates, to work with a 2D geometry, which will help to reduce the computational cost of the simulations. As for all the variables we have $\partial/\partial\phi = 0$, where ϕ is the azimuthal coordinate, we just work with the distance to the center of the droplet r and the height z. We have a dimensionless model so the geometry must be also dimensionless. We non-dimensionalize the geometry with the same dimensional factor we have use to non-dimensionalize the length in the equations, i.e., the contact radius R_c.

To mesh our geometry we use triangular elements. As the numerical problem in the gas phase is very stable (we just solve Laplace equation there) we can apply an extra coarsed mesh in this region. However, for the droplet phase, we must use an extra thin mesh. The more problematic region is near the interphase. There we refine our mesh to have 120 vertices lying along it. These nodes will move in the normal direction to the interphase following the velocity of the interphase computed through the kinematic condition. We arrive finally to a mesh with 4106 elements (see figure 3). All the solutions presented in this work have been checked to be mesh-independent in the sense that refinements in the mesh do not change the solution.

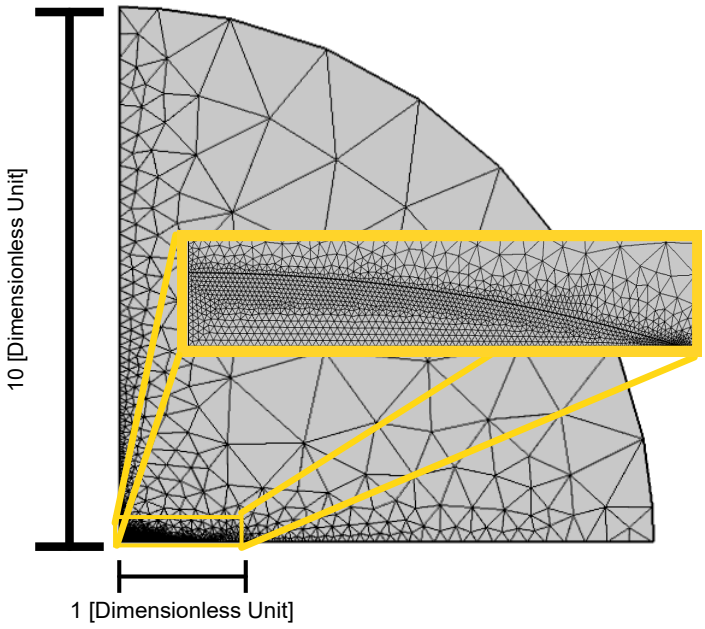

Fig. 3. Mesh applied to the geometry of the problem. A zoom is shown of the droplet domain.

To ensure numerical stability, the incompressible Stokes flow with buoyancy forces equations (52), (53) are discretized using Taylor-Hood triangular elements for pressure and velocity. In Taylor-Hood elements the velocity is approximated by a quadratic polynomial ($\mathbb{P}_2$) and the pressure by a linear polynomial ($\mathbb{P}_1$). A triangular Taylor-Hood element can be seen in figure 4.

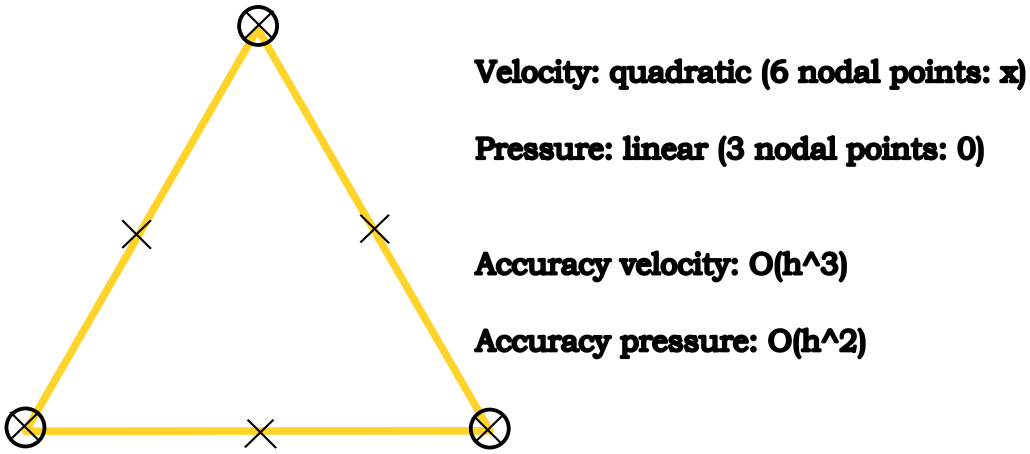

Fig. 4. Triangular Taylor-Hood element ($\mathbb{P}_2$-$\mathbb{P}_1$).

The velocity field must have a square integrable derivative and the pressure must just be square integrable in order to verify weak formulation. One can ask why we don't choose, for example, elements $\mathbb{P}_1$ for the velocity and $\mathbb{P}_0$ for the pressure. The fact that the continuity equation only contains velocity unknowns introduces some trouble.

In the stiffness matrix of the discretization the number of rows for the continuity equation is completely determined by the number of pressure unknowns. Suppose that there are more pressure unknowns than velocity unknowns. In that case the stiffness matrix contains more rows than unknowns and we have either a dependent or inconsistent system of equations that leads to a singular matrix. This is exactly what happen with element $\mathbb{P}_1$-$\mathbb{P}_0$ [13]. There is an admissibility condition that elements must fulfill. This condition is referred to as Brezzi-Babuŝka condition. It can be proved that Taylor-Hood elements verify this condition [14].

For the other equations (6), (28), (29) we use second-order polynomial $\mathbb{P}_2$ elements for the discretization, which are in the space $H^1(\Omega_G)$ and $H^1(\Omega_D)$.

9.2 ALE Method

Other important feature of the problem is the movement of the interphase that leads to deformation of the elements in the mesh. In order to handle the deformations of the elements we use the Arbitrary Lagrangian–Eulerian (ALE) method. The Eulerian method uses a fixed reference coordinate system, which implies that the nodes in the mesh are fixed and the material moves through the mesh, so it is not useful when having a free surface. Conversely, in a Lagrangian formulation, the analysis is conducted with respect to the material coordinates. The mesh is attached to the material, and it deforms and moves with the material throughout the analysis. While it excels at tracking free surfaces and material interphases, this model is not suitable for modelling large domain distortions due to the high frequency of remeshing operations it would require. See figure 5 for a graphical representation of the different approaches.
Because our model implies both large distortions of the droplet domain as well as a free surface, none of these methods are ideal. Instead of a purely Lagrangian or Eu-

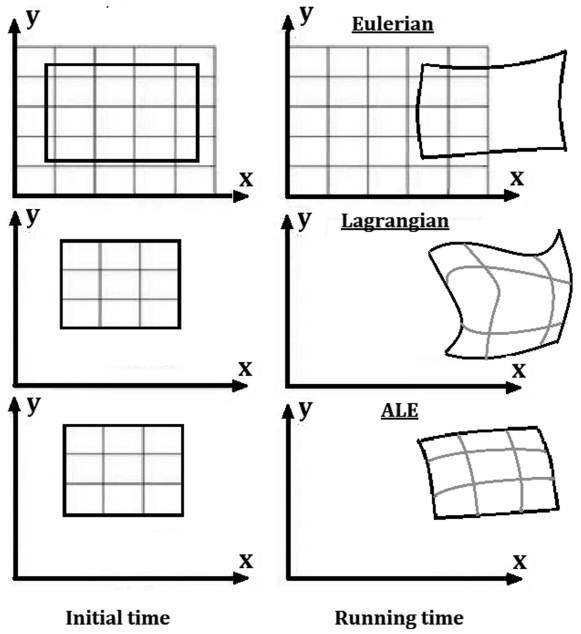

Fig. 5. Deformation of the mesh and material points from initial configuration. *Taken from* [15].

lerian approach the arbitrary Lagrangian-Eulerian (ALE) finite element formulation was chosen, as it combines the advantages of the two approaches. The displacement of the mesh elements was computed by solving a Laplace equation for the displacement field, namely $\nabla^2 \boldsymbol{q} = 0$, $\boldsymbol{q} = (q_r, q_z)$, with suitable boundary conditions. The tracking of the interphase, which is part of the solution, is done prescribing the normal velocity to the interphase, which is obtained thanks to the kinematic boundary condition (56).

9.3 Equations

The equations are introduce in the software with the Mathematical Module. In particular we use the weak form of the PDE equation. As mentioned before in Comsol we select the type of element and the order but we can not create a basis for our element that already fulfills some of the boundary conditions of our problem. For this reason we have kept our functional spaces as general as possible. We must include with Lagrange multipliers the symmetry and no-slip condition whereas the others are implicit in the weak contributions through the boundaries.

9.4 Solver

The solver must compute the time evolution of a non-linear system. For handling non-linear terms a Newton algorithm is used. The procedure is to apply a standard Newton linearization via a Taylor series expansion of nonlinear terms. Then, an iterative process is carried out, in which the linearization of the non-linear terms based on the previous solution is carried on until the convergence is ensured up to the relative tolerance.

The linear solver used is a direct fully coupled solver, this approach forms a single

large system of equations to solve simultaneously for all of the unknowns (the fields) and includes all of the couplings between the unknowns (the multiphysics effects) at once, within a single iteration. This system of equations is then directly solved. For solving the system we use a Multifrontal Massively Parallel sparse direct Solver (MUMPS) which is a solver for the solution of large sparse systems of linear algebraic equations. MUMPS implements the multifrontal method, which is a version of Gaussian elimination for large sparse systems of equations as typically arise from the finite element method.

The temporal discretization was carried out using a variable-step BDF method with 2/4 variable order. The step and order are changed to verify the relative tolerance, which was set to 10^{-4}.

10 Partial validation of the numerical strategy

In order to validate our numerical scheme we are going to use a similar, but simpler, configuration where there is an analytical solution of the problem we can compare with. This is the case of one of the first problems related with droplet evaporation, the coffee ring stain. In a seminal work from the Chicago group [16] this phenomenon was explained using the solution of the velocity field thanks to the application of lubrication theory. The application of lubrication theory is possible for small contact angle, i.e $\theta \ll 90$ °. This approximation is based on $\epsilon = h/R_c \ll 1$, which leads to a slender flow. In this approximation a solution can be found by doing a balance between capillary forces an viscous forces. The solution of the radial velocity is

$$v_r = \frac{12 D_{vap} C_s (1 - H_r)}{h^2 \pi \rho r \theta} \left(\frac{1}{\sqrt{1 - \left(\frac{r}{R_c}\right)^2}} - (1 - \left(\frac{r}{R_c}\right)^2) \right) \left(hz - \frac{1}{2} z^2 \right). \tag{76}$$

The volume evolution is

$$-\frac{\mathrm{d}V}{\mathrm{d}t} = \pi R_c f(\theta) \frac{D_{vap} C_s}{\rho} (1 - H_r), \tag{77}$$

where $f(\theta)$ is the following geometrical function

$$f(\theta) = \frac{\sin(\theta)}{1 + \cos(\theta)} + 4 \int_0^\infty \frac{1 + \cosh(2\theta\tau)}{\sinh(2\pi\tau)} \tanh[(\pi - \theta)\tau] d\tau \tag{78}$$

and the relation between the volume and the contact angle for a pinned contact line is

$$\frac{\mathrm{d}\theta}{\mathrm{d}t} = \frac{\mathrm{d}V}{\mathrm{d}t} \left(\pi R_c^3 \left(1 - \frac{\cos(\theta)(2 + \cos(\theta))(1 - \cos(\theta))^2}{\sin(\theta)^4} \right) \right)^{-1} \tag{79}$$

Then for an initial contact angle $\theta_0 \ll 90$ ° we can compare the numerical solution with the analytical one obtained through lubrication theory. It is worthy to note that this comparison is an evolutionary one, where we keep track of the interphase movement, as mentioned before, through the kinematic boundary condition and the

ALE method. For this pure water droplet the numerical problem will reduce to solve for the gas phase (6) as explained in the model and for the hydrodynamic problem (52), (53) setting Marangoni and Rayleigh number to zero, i.e $Ma = Ra = 0$. Also we set initial mass fraction of salt and protein to zero, i.e $w_{s_0} = w_{p_0} = 0$. We can compare then, for instance, the volume evolution inside the droplet, the position of the interphase, and the radial velocity (see figure 6).

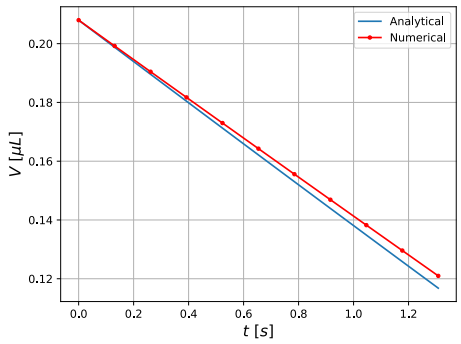

(a) Volume evolution.

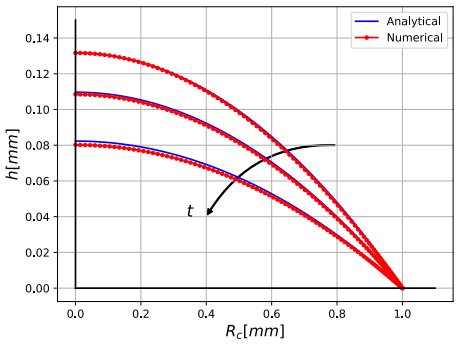

(b) interphase position.

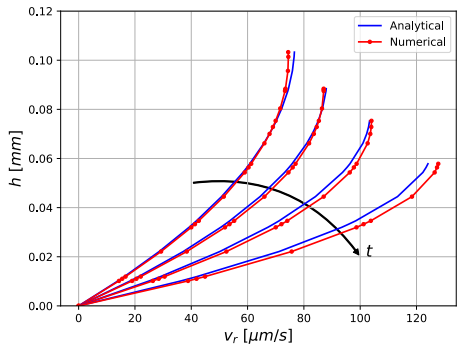

(c) Radial velocity near the center of the droplet $\frac{r}{R_c} = 0.2$.

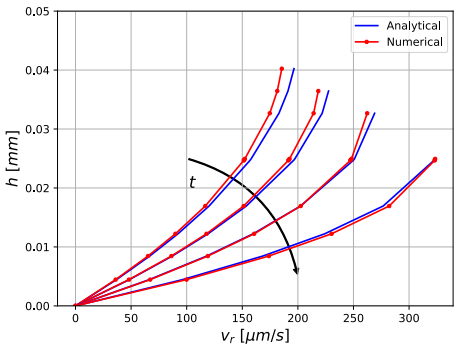

(d) Radial velocity near the contact line of the droplet $\frac{r}{R_c} = 0.8$.

Fig. 6. Analytical solution of Lubrication model versus our numerical solution.

It is important to mention that no parameters were adjusted in the numerical solution and that the error between the lubrication solution and the numerical solution is of the order of the inherent error of the lubrication model. We conclude that our numerical scheme suits evaporation of sessile droplets problems.

11 Acknowledgements

We are indebted to Ignacio González Loscertales and Javier Rivero, both from the University of Málaga, Spain, for introducing us into the modeling of free-surface problems using FEM and Comsol. In particular, many of the material shown here is based on the beautiful notes put together by Ignacio. We also want to thank Carlos de la Torre for developing an early version of the simulation tool during his bacherlor thesis. Finally, special thanks to Álvaro Marín, from UTwente, The Netherlands, for his help with the experiments and for the numerous very stimulating discussions

on the topic.

We acknowledge the funding from the Spanish MCIN/AEI/10.13039/501100011033 through Grant No. PID2020-114945RB-C21 (Experimental and theoretical study of the evaporation of expiratory droplets containing coronaviruses - Physics of the evaporation of complex droplets).

References

[1] E. P. Vejerano and L. C. Marr, "Physico-chemical characteristics of evaporating respiratory fluid droplets," *Journal of The Royal Society Interface*, vol. 15, no. 139, 2018. DOI: 10.1098/rsif.2017.0939.

[2] K. L. Chong, C. S. Ng, N. Hori, R. Yang, R. Verzicco, and D. Lohse, "Extended lifetime of respiratory droplets in a turbulent vapor puff and its implications on airborne disease transmission," *Phys. Rev. Lett.*, vol. 126, 3 Jan. 2021. DOI: 10.1103/PhysRevLett.126.034502.

[3] C. Seyfert, J. Rodríguez-Rodríguez, D. Lohse, and A. Marin, "Stability of respiratory-like droplets under evaporation," *Phys. Rev. Fluids*, vol. 7, 2 Feb. 2022. DOI: 10.1103/PhysRevFluids.7.023603.

[4] E. Mikhailov, S. Vlasenko, R. Niessner, and U. Pöschl, "Interaction of aerosol particles composed of protein and saltswith water vapor: Hygroscopic growth and microstructural rearrangement," *Atmospheric Chemistry and Physics*, vol. 4, no. 2, pp. 323–350, 2004.

[5] *Handbook of Chemistry and Physics, Internet Edition.* CRC Press, Boca Raton, FL, 2005. DOI: https://doi.org/10.1021/ja059868l.

[6] A. G. Mikos and N. A. Peppas, "Measurement of the surface tension of mucin solutions," *International Journal of Pharmaceutics*, vol. 53, no. 1, 1989. DOI: https://doi.org/10.1016/0378-5173(89)90354-2.

[7] C. Diddens, Y. Li, and D. Lohse, "Competing marangoni and rayleigh convection in evaporating binary droplets," *Journal of Fluid Mechanics*, vol. 914, 2021. DOI: 10.1017/jfm.2020.734.

[8] M. Kaneda, Y. Takao, and J. Fukai, "Thermal and solutal effects on convection inside a polymer solution droplet on a substrate," *International Journal of Heat and Mass Transfer*, vol. 53, no. 21, 2010. DOI: https://doi.org/10.1016/j.ijheatmasstransfer.2010.06.049.

[9] A. Marin, R. Liepelt, M. Rossi, and C. J. Kähler, "Surfactant-driven flow transitions in evaporating droplets," *Soft Matter*, vol. 12, 5 2016. DOI: 10.1039/C5SM02354H.

[10] L. G. Leal, *Advanced Transport Phenomena: Fluid Mechanics and Convective Transport Processes* (Cambridge Series in Chemical Engineering). Cambridge University Press, 2007.

[11] D. R. D. O. B. T. F. et al., "Capillary flow as the cause of ring stains from dried liquid drops," *Nature*, vol. 389, no. 6653, 1997. DOI: https://doi.org/10.1038/39827.

[12] *Introduction to comsol multiphysics©*. COMSOL Multiphysics, Burlington, MA., 1998.

[13] A. Segal, *Finite element methods for the incompressible Navier-Stokes equations* (Research School for Fluid Mechanics, Delft University of Technology). 2023.

[14] A. Segal, "On the numerical solution of the stokes equations using the finite element method," *Computer Methods in Applied Mechanics and Engineering*, vol. 19, no. 2, 1979. DOI: https://doi.org/10.1016/0045-7825(79)90073-2.

[15] H. Soliman, A. Shash, T. El Hossainy, and M. Abd-Rabou, "Investigation of process parameters in orthogonal cutting using finite element approaches," *Heliyon*, vol. 6, no. 11, 2020. DOI: https://doi.org/10.1016/j.heliyon.2020.e05498.

[16] R. D. Deegan, O. Bakajin, T. F. Dupont, G. Huber, S. R. Nagel, and T. A. Witten, "Contact line deposits in an evaporating drop," *Phys. Rev. E*, vol. 62, 1 Jul. 2000. DOI: 10.1103/PhysRevE.62.756.